IOP Publishing Journal of Optics
J. Opt. 19 (2017) 105301 (11pp) https://doi.org/10.1088/2040-8986/aa825d

# Quantifying external and internal collagen organization from Stokes-vector-based second harmonic generation imaging polarimetry

**Francisco J Ávila, Oscar del Barco and Juan M Bueno**

Laboratorio de Óptica, Instituto Universitario de Investigación en Óptica y Nanofísica, Universidad de Murcia, Campus de Espinardo (Ed. 34), E-30100 Murcia, Spain

E-mail: bueno@um.es

Received 7 April 2017, revised 5 July 2017
Accepted for publication 26 July 2017
Published 31 August 2017

**Abstract**

Collagen organization has been analyzed at both external and internal scales by combining Stokes-vector polarimetry and second harmonic generation microscopy. A significant linear relationship between the diattenuation and the external collagen organization was found. The dominant orientation of the collagen fibers was found to run parallel to the axis of diattenuation. Information on the collagen chirality was obtained from the circular dichroism, which showed also a strong dependence with the internal collagen organization. The results show that certain polarimetric parameters might be useful to extract quantitative information and characterize collagen arrangement.

Keywords: second harmonic generation, polarimetry, collagen, diattenuation, circular dichroism

(Some figures may appear in colour only in the online journal)

## 1. Introduction

Collagen plays an important role in maintaining the integrity of connective tissue and it is the most abundant structural protein in mammals [1]. Although there are more than 20 classified types of collagen, type-I is predominant in the human body (∼80%) [2].

Second harmonic generation (SHG) microscopy is a powerful tool to image label-free collagen-based tissues [1, 3, 4]. SHG signal originates from the basic structure of the tropocollagen molecule composed of polypeptide chains arranged in triple-helical structure [5]. These helices assemble into highly regular structures forming collagen fibrils (∼nm in diameter) [6]. The distribution of these fibrils is often understood as the internal structure of collagen. In type-I collagen tissues, these fibrils are aligned to become fibers (∼$\mu$m in size). The organization of these fibers corresponds to the external structure of the sample. The relative orientation of the fibrils within a fiber and the pitch angle of the collagen triple-helix are related to the molecular hyperpolarizability of collagen [1, 4].

SHG is a coherent nonlinear optical process that has been proved to be sensitive to polarization [1, 7]. This SHG polarization dependence provides additional information not available from intensity measurements alone, such as the ratio of hyperpolarizabilities ($\rho = \beta_{xxx}/\beta_{xyy}$) [1, 4, 7] or the molecular orientational distribution [8, 9]. Polarization-sensitive SHG has been used to better visualize the collagen fibers within a tissue and to characterize the external spatial arrangement [3, 4, 10–12]. Although collagen organization varies drastically from one tissue to another, polarization-sensitive SHG microscopy has been able to discriminate between healthy and pathological ones [13, 14]. Then, this approach provides information not only about the external distribution of collagen fibers, but also on the internal organization (i.e. both external and internal scales).

The response of SHG signal to polarization has often been analyzed in terms of linear polarized light [1, 3, 4, 7, 15]. However the use of elliptical states might provide improved SHG signal and relevant information [16–18]. Whereas the dependence of quasi-parallel collagen structures and linear polarization is well understood (theoretical and experimentally),

 

the combination of samples with non-regular arrangements and incident elliptical polarized light is still a topic of interest [12, 19]. Moreover, some polarization parameters such as the dichroic ratio [12, 20] or the anisotropy factor [21] have been defined taking into account only linear polarization. As recently reported, this fact might lead to incomplete results under certain experimental circumstances (for instance, when the specimen does not show a well-organized collagen arrangement) [19].

These drawbacks might be overpassed when using Mueller matrix polarimetry. A Mueller matrix is a $4 \times 4$ real-valued matrix containing the full polarimetric response of a sample (depolarization, birefringence and diattenuation). This matrix transforms an incident polarization state (represented by the so-called Stokes vector) into another which contains information on the polarization properties of the sample [22]. Although the Stokes–Mueller formalism is classically used in linear optics, this has been extended to SHG imaging techniques [23, 24]. Other authors have used a generalized Stokes–Mueller formalism, where the polarization properties of the sample are contained in a $4 \times 9$ matrix called double Stokes–Mueller matrix [25, 26].

On the other hand, the internal triple helices of the collagen originate intrinsic chirality [5]. This property gives rise to a different response to right- and left-handed polarized light and can be studied by measuring the circular dichroism (CD) [27]. CD has been reported to be a non-negligible optical property, which means that circular polarized light might be used to obtain information about both collagen morphology and dimensional orientation of collagen molecules [28]. Although this polarimetric property has also been used to differentiate normal tissues from diseased ones [29], in-depth analyses of the relationship between CD and the internal organization might be important to understand changes in collagen-based tissues.

Some efforts have been made to quantify the collagen properties at both external and internal scales. However, most of them have been shown to depend on a particular set of polarization states, usually linear ones, which might under- (or over-) estimate some structural properties. In that sense, a gold standard technique is required to avoid misleading conclusions. The present work uses Stokes-vector-based polarimetry to explore more precisely the dependence between diattenuation (both magnitude and axis) and the external organization of collagen-based samples. Moreover, the relationship between the collagen internal organization and the CD is also investigated.

## 2. Methods

### 2.1. Polarimetric SHG microscope and imaging procedure

The home-built multiphoton microscope used for polarimetric SHG imaging has been previously described [12]. It uses a Ti:Sapphire femtosecond laser ($\lambda_\omega = 800$ nm, 76 MHz repetition rate) as excitation source and incorporates a polarization state generator (PSG) into the illumination pathway. This PSG modulates the incoming polarization state and is composed of an horizontal polarizer and a rotatory quarter-wave ($\lambda/4$) plate. The polarized laser beam reaches the sample via a $20\times$ objective (numerical aperture, NA $= 0.5$) that is scanned in the *XY* direction. The nonlinear emission, collected via the same objective, passes a narrow-band spectral filter ($400 \pm 10$ nm) to isolate the SHG signal and it is finally detected by a photomultiplier tube.

SHG images corresponding to four independent incoming polarization states were recorded for each specimen. These states were achieved by orienting the $\lambda/4$ fast axis of the PSG at $-45°$, $0°$, $30°$ and $60°$, as described elsewhere [30]. These angles of the $\lambda/4$ plate produce left circular, linear horizontal and two elliptical polarization states, respectively. Each set of polarimetric images was used to calculate the four spatially resolved elements of elements of the first row of the Mueller matrix (see section 2.3). From these elements polarimetric parameters such as diattenuation, the axis of diattenuation and CD were computed. The image processing was performed in Matlab™.

The imaged area of each sample subtended $210 \times 210\ \mu m^2$ with a resolution of $256 \times 256$ pixels. Images were acquired at 1 Hz frame rate. The scan directions were from left to right and from top to bottom. The laser power at the sample's plane ranged between 20 and 40 mW (depending on the specimen). No photodamage was produced to the samples.

We analyzed 14 samples corresponding to non-stained ocular structures, mainly composed of type-I collagen. Sample #1 was a piece of human sclera fixed in paraffin. The rest of samples corresponded to *ex vivo* tissues (cornea and sclera) of different animals (porcine, bovine, rabbit). The former was provided by the eye bank of the Hospital Universitario Virgen de la Arrixaca, Murcia, Spain. The rest of tissues (intact ocular globes) were obtained from a local slaughterhouse and moved to the laboratory immediately after the animal's death. These were placed in a glass bottom dish filled with a phosphate buffer solution during SHG imaging. For all specimens, SHG images were acquired at layers located close to the surface. The imaged plane was always perpendicular to the axis of the microscope (to avoid tilts and minimize imaging artefacts). The experimental protocol was approved by the Universidad de Murcia ethical committee.

### 2.2. Structure tensor and collagen external organization

The external organization of a collagen sample here refers to the arrangement of the fibers (i.e. micro-scale). For its quantification the structure tensor was employed [31]. This is a representative matrix where the components are given by the partial derivatives along the Cartesian directions (*X*–*Y*). It contains information about the orientation and isotropy of every pixel within an image, which makes it appropriate to analyze the structure of collagen patterns. This tool provides several spatially resolved parameters, such as the degree of isotropy (DoI) map and the histogram of preferential orientation (PO). The structural dispersion of the analyzed sample is defined as the standard deviation of PO histogram, which is linearly correlated with the DoI. DoI ranges between 0 and 1, and as a general idea, the higher DoI, the higher the alignment of the collagen fibers along a PO. If a PO does not exist (or alternatively, DoI is close to zero), the sample is understood as a non-organized distribution of collagen fibers. To illustrate this tool, figure 1 shows an example for an artificial image.

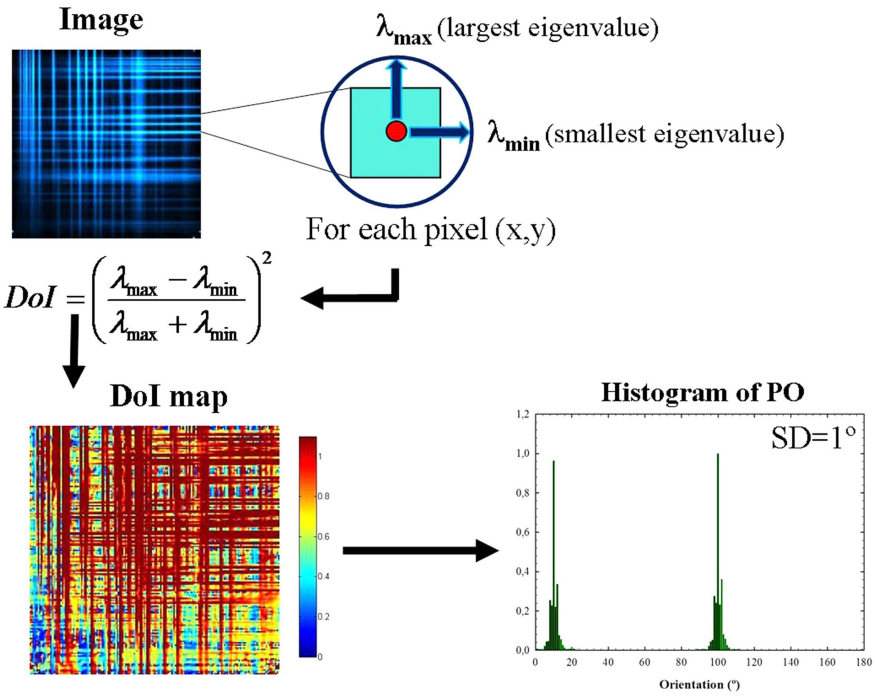


**Figure 1.** Example of the use of the structure tensor in an artificial image with two POs (at 10° and 100°). The parameter SD indicates the structural dispersion of the sample.

Further details on the mathematical formalism tensor can be found in [31].

### 2.3. Stokes–Mueller formalism and polarimetric parameters

Each independent polarization state emerging from the PSG is represented by the 4 × 1 Stokes vector $S_{\mathrm{PSG}} = [1, c, c \cdot s, s]^{\mathrm{T}}$, where $T$ indicates transposed, $c = \cos 2\alpha$, $s = \sin 2\alpha$ and $\alpha$ corresponds to the angle of the $\lambda/4$ fast axis (the four orientations above described). The laser beam passes through some optical elements of the microscope (dichroic mirror, objective, …), turning into $S_{\mathrm{IN}}^{(i)}$ ($i = 1, 2, 3, 4$) and reaching the sample under study. The sample changes this incident Stokes vector into another one, which represents the polarization state of the emitted SHG signal. For an incident polarization state $S_{\mathrm{IN}}^{(i)}$, the SHG intensity $\tilde{I}_{\mathrm{SHG}}^{(i)}$ emerging from the sample can be computed by means of:

$$\tilde{I}_{2\omega}^{(i)} = \begin{pmatrix} m_{00}^{\mathrm{SHG}} & m_{01}^{\mathrm{SHG}} & m_{02}^{\mathrm{SHG}} & m_{03}^{\mathrm{SHG}} \end{pmatrix} \cdot \begin{pmatrix} S_{0\_\mathrm{IN}}^{(i)} \\ S_{1\_\mathrm{IN}}^{(i)} \\ S_{2\_\mathrm{IN}}^{(i)} \\ S_{3\_\mathrm{IN}}^{(i)} \end{pmatrix} = MC_{\mathrm{SHG}} \cdot S_{\mathrm{IN}}^{(i)}, \quad (1)$$

where $MC_{\mathrm{SHG}}$ is a 1 × 4 vector containing the sample's properties responsible for the changes in the emitted SHG intensity. Further information and more details on this formalism can be found in the appendix.

The four elements of $MC_{\mathrm{SHG}}$ are the unknowns in equation (1). Then, to compute those elements four incident polarization states $S_{\mathrm{IN}}^{(i)}$ are required. Defining $MS_{\mathrm{IN}}$ as a 4 × 4 auxiliary matrix which columns are those Stokes vectors, equation (1) can be rewritten as:

$$\begin{aligned} MI_{\mathrm{SHG}} &= \begin{pmatrix} \tilde{I}_{\mathrm{SHG}}^{(1)} & \tilde{I}_{\mathrm{SHG}}^{(2)} & \tilde{I}_{\mathrm{SHG}}^{(3)} & \tilde{I}_{\mathrm{SHG}}^{(4)} \end{pmatrix} \\ &= MC_{\mathrm{SHG}} \cdot \begin{pmatrix} S_{0\_\mathrm{IN}}^{(1)} S_{0\_\mathrm{IN}}^{(2)} S_{0\_\mathrm{IN}}^{(3)} S_{0\_\mathrm{IN}}^{(4)} \\ S_{1\_\mathrm{IN}}^{(1)} S_{1\_\mathrm{IN}}^{(2)} S_{1\_\mathrm{IN}}^{(3)} S_{1\_\mathrm{IN}}^{(4)} \\ S_{2\_\mathrm{IN}}^{(1)} S_{2\_\mathrm{IN}}^{(2)} S_{2\_\mathrm{IN}}^{(3)} S_{2\_\mathrm{IN}}^{(4)} \\ S_{3\_\mathrm{IN}}^{(1)} S_{3\_\mathrm{IN}}^{(2)} S_{3\_\mathrm{IN}}^{(3)} S_{3\_\mathrm{IN}}^{(4)} \end{pmatrix} \\ &= MC_{\mathrm{SHG}} \cdot MS_{\mathrm{IN}}. \end{aligned} \quad (2)$$

In particular, for the present experiment, the elements of the 1 × 4 vector $MI_{\mathrm{SHG}}$ are the four experimentally recorded SHG images, one for each incident polarization state. In this sense, the unknown spatially resolved elements of $MC_{\mathrm{SHG}}$ (or the pixel-by-pixel values of the four elements of $MC_{\mathrm{SHG}}$) can be finally computed as:

$$MC_{\mathrm{SHG}} = MI_{\mathrm{SHG}} \cdot (MS_{\mathrm{IN}})^{-1}. \quad (3)$$

It is worth mentioning that the 4 × 4 matrix $MS_{\mathrm{IN}}$ does have an inverse because its determinant is different from zero. These polarization states are mathematically independent as it was corroborated in a previous calibration operation using an auxiliary polarization analyzer composed of a $\lambda/4$, a linear polarizer and a photodetector (see for instance [32] for further details on the polarimetric calibration).

Once the elements of $MC_{\mathrm{SHG}}$ are known, the sample's diattenuation map (i.e. the spatially resolved diattenuation

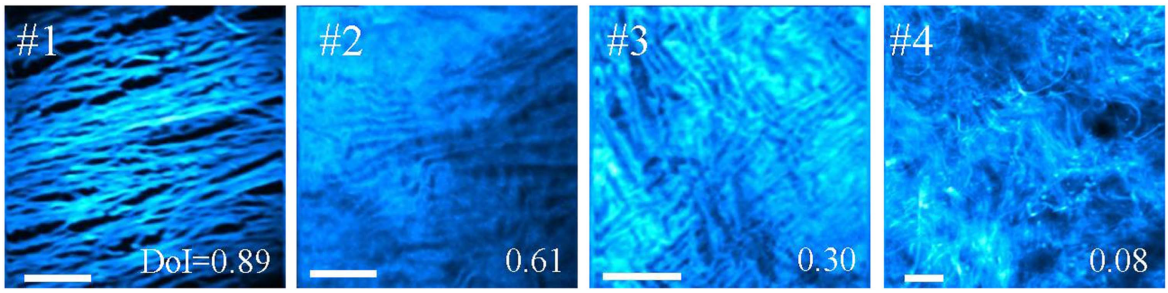


**Figure 2.** Experimental SHG images corresponding to a human sclera (fixed in paraffin, #1), *ex vivo* bovine (#2) and porcine (#3) corneas, and a piece of human sclera (#4). Scale bar: 50 $\mu$m.

values) can be computed as [22]:

$$D = \frac{\sqrt{(m_{01}^{\mathrm{SHG}})^2 + (m_{02}^{\mathrm{SHG}})^2 + (m_{03}^{\mathrm{SHG}})^2}}{m_{00}^{\mathrm{SHG}}}, \tag{4}$$

which ranges between 0 and 1. This parameter is often referred to as polarization sensitivity, that is, the dependence between the intensity emerging from an optical system and the polarization state of the incident beam. For a given $MC_{\mathrm{SHG}}$ the maximum and minimum intensity values, $\tilde{I}_{\mathrm{SHG}}^{(\max)}$ and $\tilde{I}_{\mathrm{SHG}}^{(\min)}$, are defined as:

$$\begin{aligned} \tilde{I}_{\mathrm{SHG}}^{(\max)} &= m_{00}^{\mathrm{SHG}} + \sqrt{(m_{01}^{\mathrm{SHG}})^2 + (m_{02}^{\mathrm{SHG}})^2 + (m_{03}^{\mathrm{SHG}})^2}, \\ \tilde{I}_{\mathrm{SHG}}^{(\min)} &= m_{00}^{\mathrm{SHG}} - \sqrt{(m_{01}^{\mathrm{SHG}})^2 + (m_{02}^{\mathrm{SHG}})^2 + (m_{03}^{\mathrm{SHG}})^2} \end{aligned} \tag{5}$$

and the Stokes vector providing this $\tilde{I}_{\mathrm{SHG}}^{(\max)}$ will be given by:

$$S_{\max} = \frac{1}{m_Q} \cdot \begin{pmatrix} m_Q \\ m_{01}^{\mathrm{SHG}} \\ m_{02}^{\mathrm{SHG}} \\ m_{03}^{\mathrm{SHG}} \end{pmatrix} \quad \text{with}$$

$$m_Q = \sqrt{(m_{01}^{\mathrm{SHG}})^2 + (m_{02}^{\mathrm{SHG}})^2 + (m_{03}^{\mathrm{SHG}})^2}. \tag{6}$$

As a consequence, the axis of diattenuation lies parallel to $S_{\max}$ and it can be computed as [33]:

$$\mathrm{Axis}_D = \frac{1}{2} \cdot \arctan\left(\frac{m_{02}^{\mathrm{SHG}}}{m_{01}^{\mathrm{SHG}}}\right). \tag{7}$$

On the other hand, as the dichroic ratio of a material is defined as the ratio between $\tilde{I}_{\mathrm{SHG}}^{(\max)}$ and $\tilde{I}_{\mathrm{SHG}}^{(\min)}$, it can be expressed as a function of diattenuation as [34]:

$$DR = \frac{\tilde{I}_{\mathrm{SHG}}^{(\max)}}{\tilde{I}_{\mathrm{SHG}}^{(\min)}} = \frac{1+D}{1-D}. \tag{8}$$

The CD is the differential absorption of left- ($\tilde{I}_{\mathrm{SHG}}^{CL}$) and right- ($\tilde{I}_{\mathrm{SHG}}^{CR}$) handed polarized light. Then, it can be defined as the contrast of intensities for circular polarized light [29] and in terms of the elements of $MC_{\mathrm{SHG}}$ CD can be directly computed as:

$$\mathrm{CD} = \frac{\tilde{I}_{\mathrm{SHG}}^{CR} - \tilde{I}_{\mathrm{SHG}}^{CL}}{(\tilde{I}_{\mathrm{SHG}}^{CR} + \tilde{I}_{\mathrm{SHG}}^{CL})/2} = 2 \cdot \frac{m_{03}^{\mathrm{SHG}}}{m_{00}^{\mathrm{SHG}}}. \tag{9}$$

## 3. Results

### 3.1. Diattenuation and external organization

As an example, figure 2 shows SHG images of different ocular tissues involved in the present work: sclera (#1, #4) and cornea (#2, #3). The samples were chosen to be representative of different external arrangement patterns. For the sense of completeness, the averaged values of DoI are also presented. As expected, it is readily observable that the highest DoI value corresponds to the specimen with a higher collagen organization. In particular, DoI values indicate that sample #1 is well-organized (DoI $\geqslant$ 0.7), #2 and #3 are partially organized samples (0.7 $>$ DoI $\geqslant$ 0.20), and #4 is a sample with a non-organized distribution (DoI $<$ 0.20) [31].

Figure 3 shows two sets of polarimetric SHG images corresponding to samples #2 and #4 (one SHG image for each incident polarization state, as indicated). For each set of four polarimetric SHG images, the elements of the corresponding $MC_{\mathrm{SHG}}$ vector were computed using the procedure above described. The four spatially resolved elements of $MC_{\mathrm{SHG}}$ computed from the images in figure 3 are given in figure 4. Since the values of the elements of $MC_{\mathrm{SHG}}$ are different from zero, some dependence between the intensity of the SHG images and the incident polarization state is expected.

Once the elements of $MC_{\mathrm{SHG}}$ are known, the map of diattenuation can be obtained by using equation (4). This map shows the pixel-by-pixel sensitivity of the sample to the incident polarization. At this point and taking this into account, the question would be: is this dependence with polarization related to the external structure of the collagen-based sample? To answer this question, we have compared the DoI maps computed through the structure tensor (section 2.2) with the maps of diattenuation. As representative examples, figure 5 presents those maps for samples #2 and #4. The averaged values across the images have been included for clarity.

Moreover, both spatially resolved parameters (i.e. diattanuaiton and DoI) have been computed for the 14 different samples involved in the present experiment. Figure 6 depicts the relationship between diattenuation and DoI values. The plot confirms that diattenuation significantly increases with the external organization. That is, a sample with a higher DoI presents higher diattenuation (i.e. higher polarization

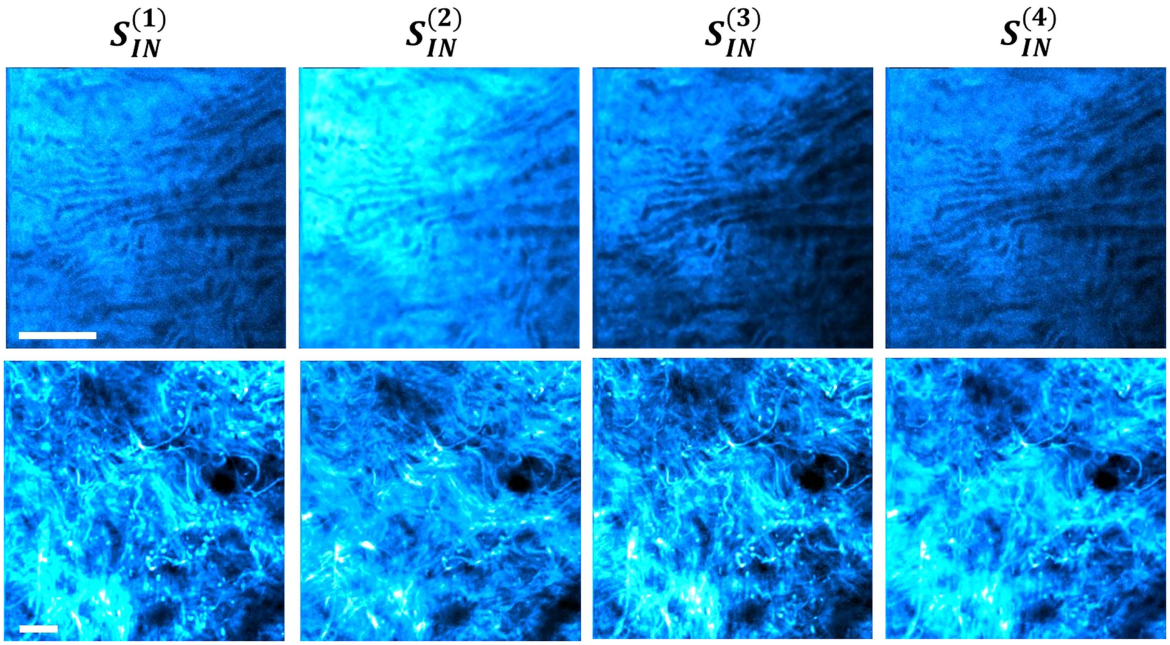


**Figure 3.** Polarimetric SHG images for sample #2 (upper panels) and #4 (bottom panels). Each image was acquired with a different incident polarization state (see labels at the top of each image). Scale bar: 50 $\mu$m.

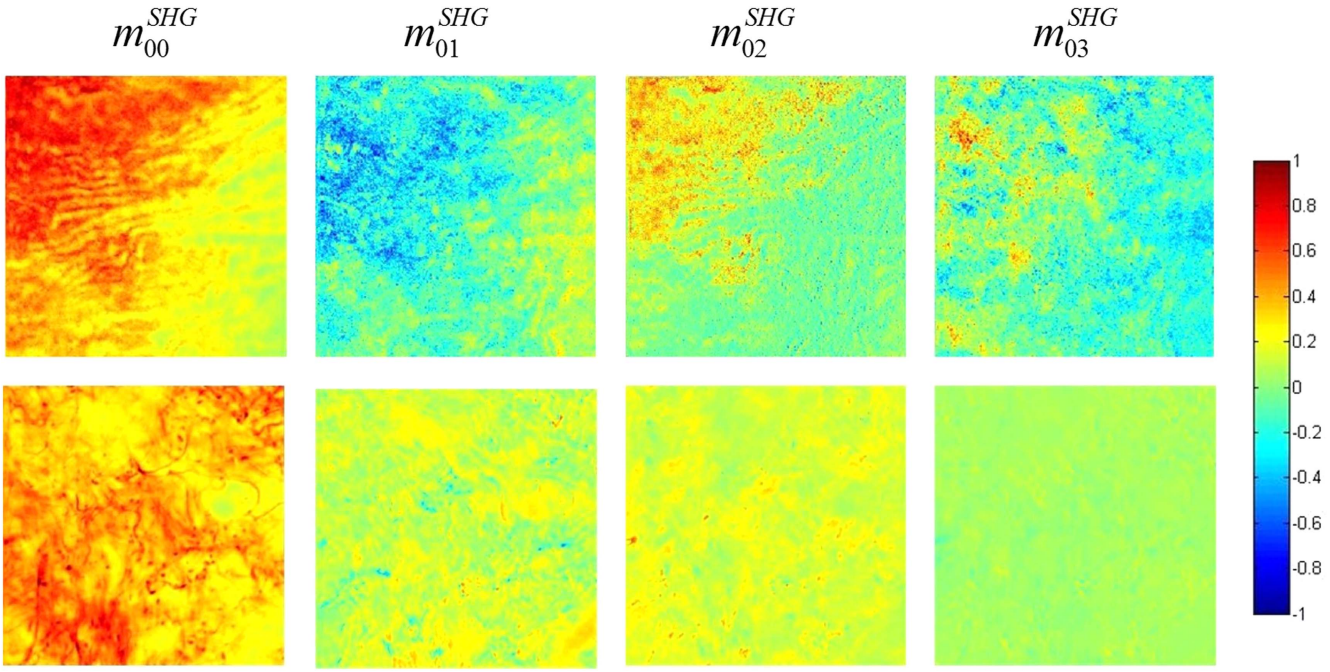


**Figure 4.** Spatially resolved elements of the $MC_{\mathrm{SHG}}$ vector computed from the images of figure 3. Color level code is shown at the right.

sensitivity). These data can be fitted to a linear function ($R^2 = 0.88$ and $p < 0.0001$).

The maps of $\mathrm{Axis}_D$ have been computed from the elements of the vector $MC_{\mathrm{SHG}}$ by means of equation (7). Figure 7 shows these maps for samples #1 (quasi-parallel distribution) and #2 (partially aligned). The mean value across each map is also shown. The PO histograms calculated with the structure tensor for the same specimens are also presented. It is interesting to notice that the mean values obtained for $\mathrm{Axis}_D$ and PO are similar. This indicates a close correlation between the preferential direction of the collagen fibers (if any) and the axis of diattanuation of the sample. For the sense of completeness, figure 8 compares the $\mathrm{Axis}_D$ and the corresponding PO for eight different samples. This correlation can only be established in samples with quasi-parallel and partially organized arrangement. The rest of samples (6 out of 14) have not been included in the plot since they correspond to non-organized structures and the PO histograms did not present a preferred direction of the fibers [31]. A significant linear correlation between these two

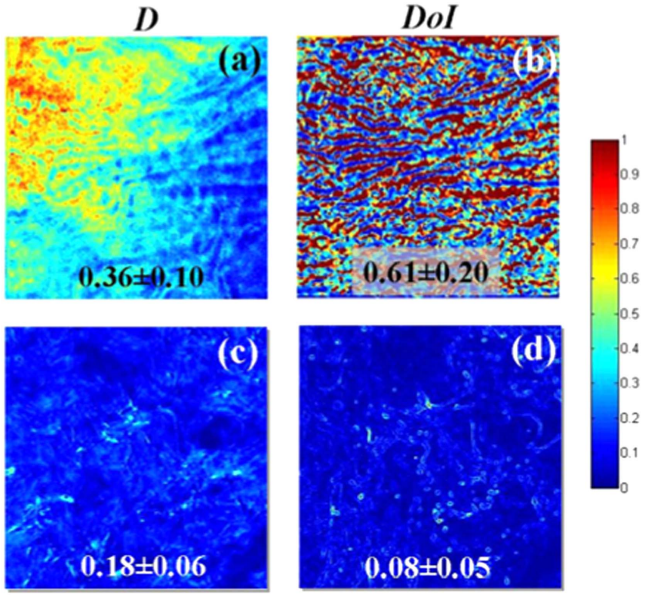


**Figure 5.** Maps of $D$ (left panels) and DoI (right panels) corresponding to samples #2 (upper row) and #4 (bottom row). The color bar is shown at the right.

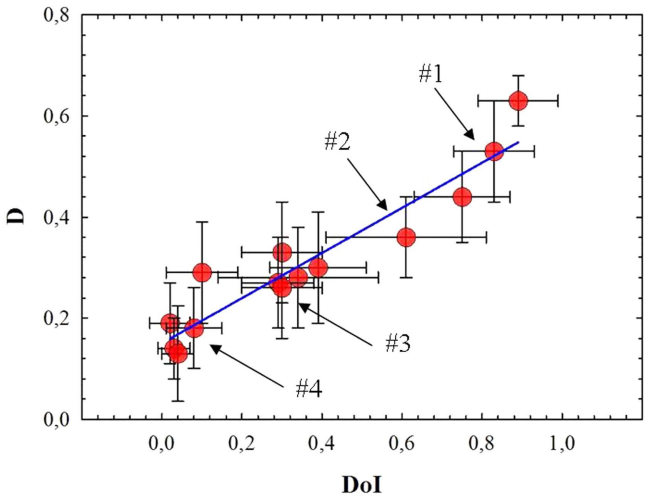


**Figure 6.** Relationship between DoI and diattenuation for 14 different collagen-based samples. A significant linear correlation was found ($D = 0.45 \cdot \mathrm{DoI} + 0.15$). The samples of figure 2 have been labeled. Error bars indicate the standard deviation.

parameters was also found ($R^2 = 0.99$ and $p < 0.0001$): $\mathrm{Axis}_D = 1.05 \cdot \mathrm{PO} - 0.79$.

### 3.2. Diattenuation: experiment versus theory

In order to corroborate the performance of the numerical model presented in the appendix for all samples used here, figure 9 depicts the comparison between the experimental values of $D$ (already shown in figure 6) and the theoretical ones. Equation (4) was also used to compute the theoretical $D$ values. The elements $m_{0i}^{\mathrm{SHG}}$ ($i = 0, 1, 2, 3$) involved in this equation (4) were obtained from the numerical calculation of the vector $MC_{\mathrm{SHG}}$ in equation (A4) of the appendix. Results reveal a statistical significant linear correlation ($R^2 = 0.90$ and $p < 0.0001$). The agreement between both sets of data can be noticed in this plot. This corroborates the fairly good accuracy of the theoretical model and justifies the assumption of Kleinman symmetry (see the appendix for more information on this).

### 3.3. CD and internal organization

It has been recently reported that there exists a parabolic dependence between the ratio of hyperpolarizabilities, $\rho$, and the external organization of the sample measured as the structural dispersion (or alternatively the DoI, since they are linearly correlated [12]). However the values of $\rho$ were experimentally computed from the dichroic ratio, defined as the ratio of the intensities for horizontal and vertical linear polarizations, $\mathrm{DR}_{\mathrm{HV}} = I_{\mathrm{H}}/I_{\mathrm{V}} = \rho^2$ [12, 20]. This definition 'only' takes into account the linear polarized light that might lead to some discrepancies as very recently stated [19]. To test if the relationship is still valid when using the generalized expression of the DR (equation (8)) computed from the elements of the Mueller matrix, figure 10 compares the values of DoI and $\rho$ for all the specimens. Once again the plot shows that both parameters are related through a parabolic function ($R^2 = 0.91$, $p < 0.0001$).

From figure 10, it can be seen that the calculation of $\rho$ is incomplete since the present results yield only the magnitude of $\rho$ but not the sign. This issue was also present when using linear polarized light and it was solved by using the information of the SHG intensity corresponding to an additional linear polarization state (at 60°) [18]. However, that solution did not provide information on the physical properties associated to the sign of $\rho$, which might be relevant for the internal characterization of the collagen structure. As will be shown in the following, the sign of $\rho$ can be related to the properties of CD, that is, to the intrinsic chirality of the collagen [27, 28].

The values of CD can be computed pixel-by pixel via equation (9). As an example, figure 11 presents the maps of CD for two samples together with the mean values across the images. It can be observed that CD has negative values. The partially-organized sample (#2) presents also a higher CD (in absolute value) than the non-organized one (sample #4). This fact can be better seen in figure 12.

Figure 12(a) presents the CD as a function of $\rho$ for the 14 different collagen-based samples used along this work. The behavior of $\rho$ shows some symmetry around $\mathrm{CD} = 0$. Although the best fit of this data corresponds to the function 'absolute value', a graphical relationship is not enough to justify the sign of $\rho$. To confirm that a negative $\rho$ value is associated with a negative CD value (and $\rho > 0$ with $\mathrm{CD} > 0$), for each specimen we used the additional polarimetric image reported in [18]. The acquired polarimetric SHG image provided us the sign of $\rho$. It is verified that if a sample presents a positive value of $\rho$, the CD computed from equation (9) is also positive (and vice versa). Having taken this into account, figure 12(b) depicts the same data as in figure 12(a) with the values of $\rho$ with the correct sign. There is a significant linear correlation ($R^2 = 0.97$, $p < 0.0001$)

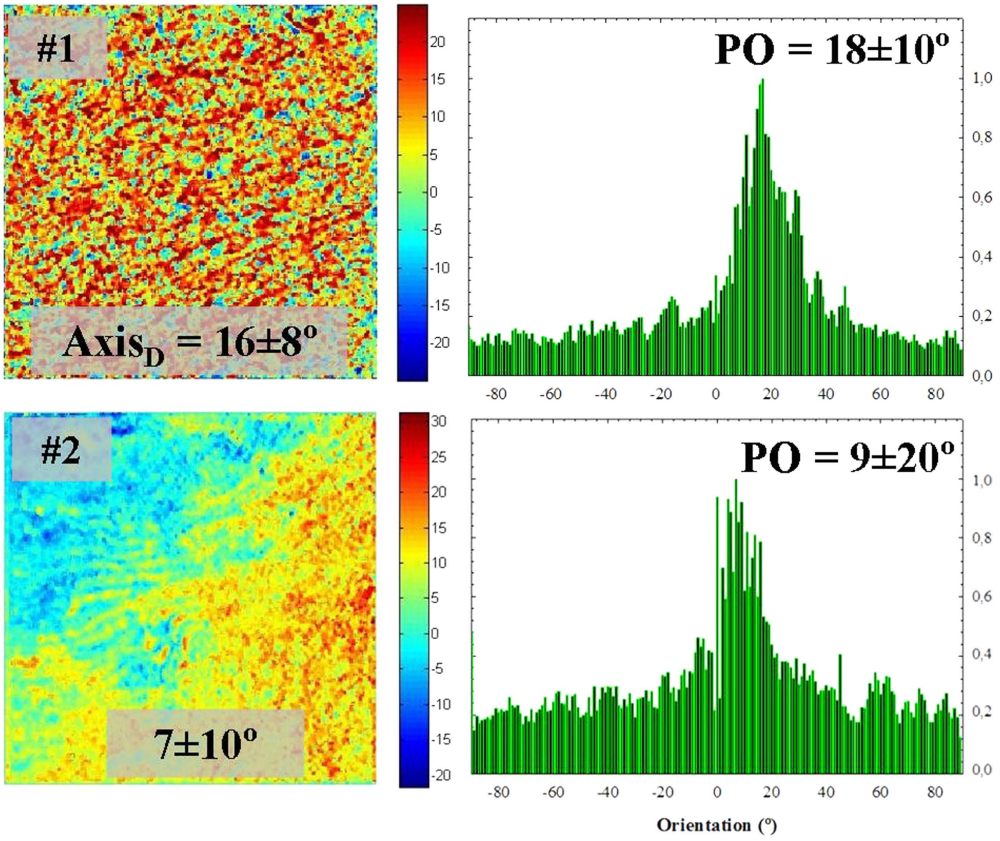


**Figure 7.** Spatially resolved Axis$_D$ and PO distribution histograms of samples #1 and #2.

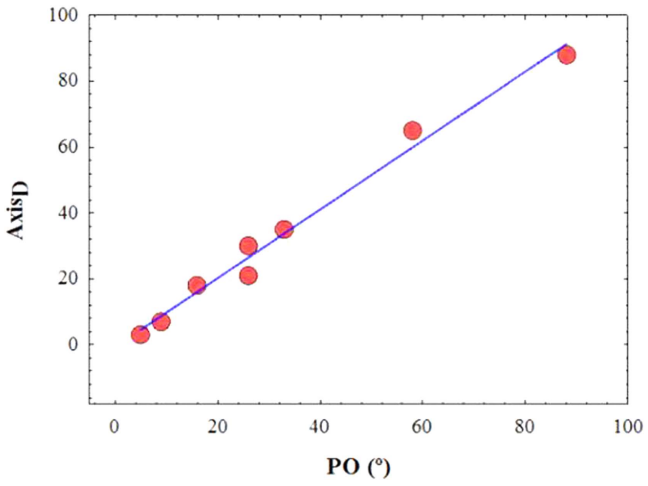


**Figure 8.** Dependence between Axis$_D$ and PO for eight different samples. The values are the mean across the maps. The blue line corresponds to the best linear correlation ($R^2 = 0.99$, $p < 0.0001$).

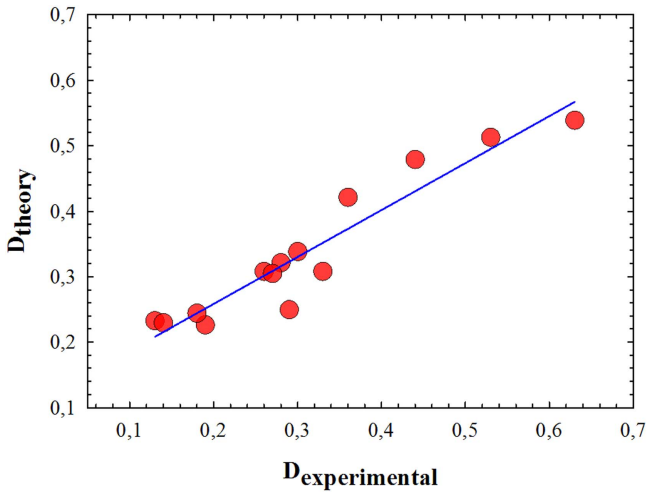


**Figure 9.** Experimental versus theoretical $D$ values for the different collagen-based samples used in this work. For the theoretical model $\lambda_\omega = 800$ nm and an objective numerical aperture of 0.50.

between both parameters, which provides a direct method to obtain the sign of $\rho$ directly from the sign of CD.

## 4. Discussion and conclusions

A polarimetric SHG imaging microscope has been used to further explore the external and internal organization of collagen-based samples. Four SHG images corresponding to independent polarization states were used to compute four Mueller matrix spatially resolved elements. Since this matrix can fully characterize the polarization response of any sample [22], some polarimetric parameters such as diattenuation, dichroic ratio and CD were computed. These parameters were used to obtain additional quantitative information on structure of the analyzed specimens.

In the last few years, there has been an increasing interest in quantifying external collagen fiber organization from SHG

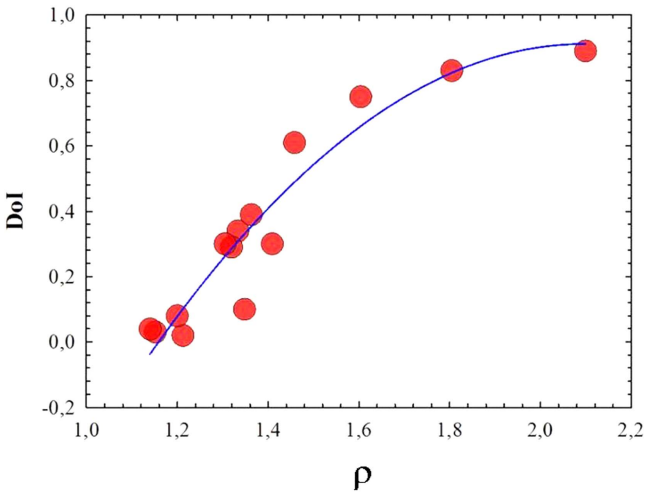


**Figure 10.** Relationship between DoI and $\rho$ for all samples involved in this study. A parabolic function was the best fitting between both parameters ($\mathrm{DoI} = -\rho^2 + 4.35 \cdot \rho - 3.65$).

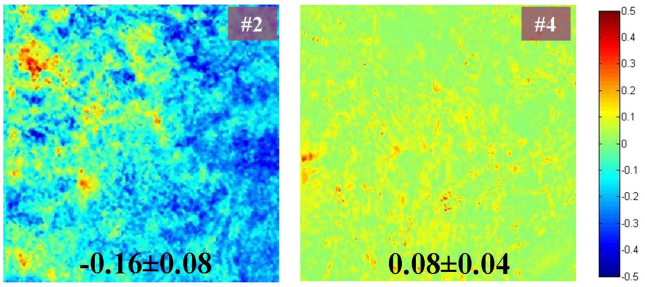


**Figure 11.** Maps of CD for samples #2 and #4.

images. Although Fourier analyses have often been used [35], a recent study has successfully applied the structure tensor to classify different collagen patterns according to their organization [31]. This structure tensor is the approach used in this paper.

Diattenuation contains global information relative to the polarization sensitivity of a sample. In the present work, the SHG intensity depends on the elements the vector $MC_{\mathrm{SHG}}$. If those elements are null, there is no dependence between the SHG intensity and the incoming polarization state. This is not the case here, and diattenuation parameter computed from $MC_{\mathrm{SHG}}$ is also different from zero, ranging between 0.12 and 0.63 for the samples involved in this study. These values have shown a significant linear correlation with the external distribution of fibers (figure 6): the higher (lower) the DoI, the higher (lower) the diattenuation. Although this linear correlation has not been reported previously, it is not surprising. It is well known that SHG signal emerging from a sample is polarization dependent. Moreover, it has also been reported that the modulation of the SHG signal for linear polarization is maximized when the sample under study presents a quasi-parallel external structure, that is DoI values >0.70 [12]. When the sample presents a lower external organization (i.e. DoI decreases), this modulation is reduced. Taking into account that diattenuation represents the sensitivity to incident polarization, this fact has been further explored here. Through the use of the diattenuation parameter we have demonstrated that this polarization dependence is a general behavior and it does not depend on the relative angle between the collagen fibers and the excitation polarization state used for imaging (often linear in earlier works [10, 19]).

This non-null value of diattenuation gives place to $\tilde{I}_{\mathrm{SHG}}^{(\mathrm{max})}$ and $\tilde{I}_{\mathrm{SHG}}^{(\mathrm{min})}$ (equation (5)). The $\mathrm{Axis}_D$ (calculated using equation (7)) is the azimuth of the incident Stokes vector providing $\tilde{I}_{\mathrm{SHG}}^{(\mathrm{max})}$. As expected from the elements of $MC_{\mathrm{SHG}}$, the $\mathrm{Axis}_D$ maps were not uniform. Despite this, the averaged $\mathrm{Axis}_D$ value across each map was similar to the PO of the fibers computed from the structure tensor (see figure 6), that is, PO and $\mathrm{Axis}_D$ presented a linear relationship (figure 8). This means that there is a strong 'biological structural link' between the dominant orientation of the collagen fibers and the direction of maximum SHG intensity. It is worth mentioning that this only occurred with quasi-aligned and partially aligned samples, since PO did not exist for non-organized specimens [31].

This finding might be important in some cases where the SHG signal from the sample is very low and could be increased by selecting an appropriate polarization state for the illumination laser beam. This agrees with a recent study by Hristu *et al* [19], where they report a novel methodology to select an optimal incident polarization to characterize tissues (and also differentiate healthy from pathological ones) using the anisotropy factor and Fourier analyses.

Combining Mueller matrix polarimetry and SHG imaging, Bancelin *et al* reported that the dominant orientation of the fibers uterine cervical tissue was similar to the axis of both diattenuation and birefringence [24]. This is coherent with the results presented here (for 14 different samples), since the $\mathrm{Axis}_D$ was found to be collinear and aligned along the main orientation of collagen fibers.

SHG polarimetry was also used to explore birefringence [11, 24, 36] or the degree of polarization [23, 25, 37]. Although it is not the scope of this paper, the experimental setup reported here might be used to analyze those polarization properties if an analyzer unit is placed in front of the recording unit.

It is well know that internal collagen spatial distribution can be quantified by means of the ratio of hyperpolarizabilities, $\rho$. This parameter has been shown to be vary between $-3$ and $+3$ [1, 15] and it decreases with the loss of regular distribution and collagen aging [1, 3, 15, 17, 38]. Although in some references only the absolute values of $\rho$ are presented (see for instance [7] and [39]), both magnitude and sign are thought to be important for a complete internal collagen characterization. A recent study has experimentally determined the parameter $\rho$ from three experimental values of the SHG intensity corresponding to incident linearly polarized light [18]. However, since the response of collagen-based structures to polarization strongly depends on their organization, the use of only this type of polarized light might have some influence on the results and reduce its accuracy [19].

In this work, the ratio $\rho$ has been computed from the dichroic ratio, defined from the diattenuation (equation (8)) and not from the SHG intensities corresponding to linear polarized light. Similarly to the diattenuation, the dichroic ratio (or

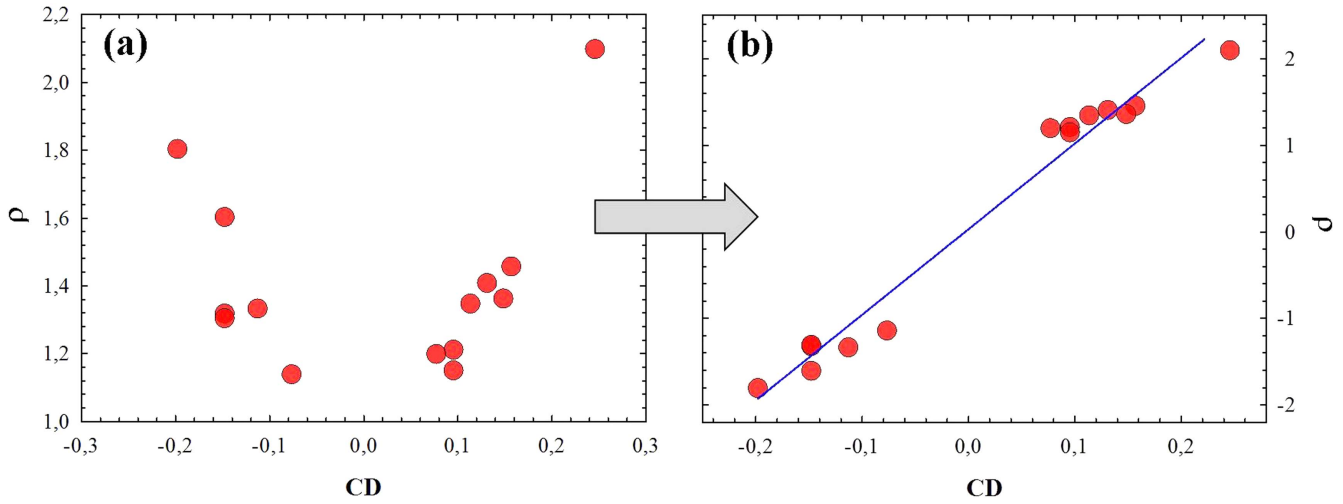


**Figure 12.** Relationship between the circular dichroism CD and the ratio of hyperpolarizabilities before (a) and after (b) computing the corresponding sign.

alternatively $\rho$) was also found to depend on the DoI, but instead of a linear relationship, a parabolic one was the best fit. This result agrees with that reported in [12], although the present case can be understood as a generalization, due to this 'global' definition of DR. However, this calculation of $\rho$ is partial since only the module is known (see figure 10). In order to calculate its sign, the concept of CD was introduced.

Together with $\rho$, the CD is another property closely related to the internal properties of collagen, in particular chirality [27]. To investigate the dependence between both parameters, the CD was computed from equation (9) for all the samples involved in this study. As expected from the spatial distribution of elements $m_{03}^{\mathrm{SHG}}$ and $m_{00}^{\mathrm{SHG}}$, the maps of CD were not uniform and presented both positive and negative values. The relationship between the module of $\rho$ and CD was fit by an absolute value function (see figure 12(a)). This experimental finding indicates that CD and $\rho$ present the same sign (figure 12(b)), which avoids the use of an extra polarimetric image [18]. It is worth remembering that the CD is proportional to the ratio between $m_{03}^{\mathrm{SHG}}$ and $m_{00}^{\mathrm{SHG}}$. Since the latter represents the intensity when non-polarized light is incident and it is always positive, the sign of the CD can be directly determined by the sign of the element $m_{03}^{\mathrm{SHG}}$. That is, samples with CD $< 0$ will also have $\rho < 0$.

The linear dependence between CD and $\rho$ indicates that a high internal (i.e. molecular) collagen organization (or alternatively, high $/\rho/$) is associated with a high value of |CD|. It has been reported that, whereas CD is close to zero for a complete denatured protein, a properly folded protein has a non-vanishing CD [29]. The present results agree well with this fact, since samples with denatured collagen present low values of the ratio $/\rho/$ [1, 3, 11, 15, 38] and these are related to low values of |CD|. In addition, structural changes of collagen due to misfoldings of the triple helices would also lead to a decrease in $/\rho/$ (as occurs in severe diseases [40]).

Our results are consistent with those reported by Lee and co-workers [28]. They showed that the CD obtained from SHG microscopy provides molecular information on collagen fibers [28]. They also claimed that the sign of the CD depends on the orientation of the longitudinal axis of the collagen triple helix, so that they can interpret the axial orientation of local collagen molecules from CD measurements. Since a change in the sign of the ratio $\rho$ suggests a reversed polarity [15, 41], a possible explanation for the relationship between the sign of CD and $\rho$ is that changes in the directionally of the molecules axis are closely linked to variations in the induced SHG dipole moments [15, 17].

In conclusion, Stokes-vector-based polarimetry has been combined with SHG imaging microscopy to quantify the collagen organization at both external and internal scales. It has been shown that collagen-based tissues behave as diattenuators with the axis parallel to the preferred orientation of the fibers. Diattenuation was found to have a linear dependence with the external organization, which means that a sample with a high structural dispersion of the collagen fibers has low polarization sensitivity. CD presented a significant correlation with the internal collagen structure (measured through the parameter $\rho$), which indicates that the chirality of collagen molecules is strongly related to the organization of the collagen fibrils. Since the mechanical effects, trauma and disease can modify collagen arrangement at both scales, this approach allows an integral measurement and collagen characterization that might help in early diagnosis or tracking of pathologies.

## Acknowledgments

Supported by Secretaría de Estado de Investigación, Desarrollo e Innovación (SEIDI), Spain (grant FIS2016-76163-R).

## Appendix

### *Theoretical Stokes–Mueller formalism for SHG signal in collagen fibers*

In terms of SHG processes, the polarization properties of a sample can be described by the 4 × 9 double Stokes–Mueller

matrix. Similarly to linear optics, in polarimetric terms, the elements of the first row of this matrix are responsible for the dependence between the SHG signal emerging from the sample and the polarization state of the incident light. However, this general double Stokes–Mueller matrix can be noticeable simplified assuming both Kleinman and cylindrical symmetries in collagen-based samples [26]. This is very interesting since five out of nine elements of the first row of the matrix become zero. Only the elements $m_{0i}^{\mathrm{SHG}}$ ($i = 0, 1, 2, 3$) remain non-null. For the sense of completeness, these non-null elements are numerically computed along this appendix.

For this aim, let us consider an elliptically polarized light (azimuth $\chi$, ellipticity $\psi$ and phase difference $\delta$) with wavelength $\lambda_\omega$ represented by its Stokes vector $S_{\mathrm{IN}}$. If this light beam is incident on a sample composed of N collagen fibers with a certain structural dispersion [12], the emerging SHG intensity $\tilde{I}_{2\omega}$ will be a result of:

$$\tilde{I}_{2\omega} = \begin{pmatrix} m_{00}^{\mathrm{SHG}} & m_{01}^{\mathrm{SHG}} & m_{02}^{\mathrm{SHG}} & m_{03}^{\mathrm{SHG}} \end{pmatrix} \cdot \begin{pmatrix} S_{0\_\mathrm{IN}} \\ S_{1\_\mathrm{IN}} \\ S_{2\_\mathrm{IN}} \\ S_{3\_\mathrm{IN}} \end{pmatrix} = MC_{\mathrm{SHG}} \cdot S_{\mathrm{IN}}, \tag{A1}$$

where $MC_{\mathrm{SHG}}$ is a $1 \times 4$ vector containing the sample's properties responsible for the changes in the emitted SHG intensity. In polarization theory, this vector is equivalent to the first row of the Mueller matrix (four elements), containing information on diattenuation. This SHG intensity $\tilde{I}_{2\omega}$ can be expressed as (see [17] and [18] for specific details):

$$\tilde{I}_{2\omega} \approx A(\theta, \Phi) \cdot B(\lambda_\omega, \mathrm{NA}) \cdot C(\chi, \psi, \beta_{xxx}, \beta_{xyy}). \tag{A2}$$

In this equation, the term $A$ contains the spatial dependence ($(\theta, \Phi)$ are the angular coordinates in the backward direction, i.e. $\pi/2 < \theta < 3\pi/2$), and the term $B$ depends on $\lambda_\omega$, and the NA of the objective. Apart from $\chi$ and $\psi$, the term $C$ also includes the two non-null elements (under both Kleinman and cylindrical symmetries) of the second-order hyperpolarizability tensor, $\beta_{xxx}$ and $\beta_{xyy}$. This tensor is related to the SHG dipole moment induced by the collagen fibers [15, 17]. In particular, this last term is the only one containing polarization information and is given by:

$$\begin{aligned} C(\chi, \psi, \beta_{xxx}, \beta_{xyy}) = {} & \cos^4\psi((\beta_{xxx}\cos^2\chi + \beta_{xyy} \\ & \times \sin^2\chi)^2 + \beta_{xyy}^2 \sin^2(2\chi)) \\ & + \sin^4\psi((\beta_{xxx}\sin^2\chi + \beta_{xyy} \\ & \times \cos^2\chi)^2 + \beta_{xyy}^2 \sin^2(2\chi)) \\ & + \frac{1}{2}\sin^2(2\psi)\cos(2\delta)((\beta_{xxx} \\ & \times \cos^2\chi + \beta_{xyy}\sin^2\chi)(\beta_{xxx} \\ & \times \sin^2\chi + \beta_{xyy}\cos^2\chi) \\ & - \beta_{xyy}^2 \sin^2(2\chi)). \end{aligned} \tag{A3}$$

In order to compute the four unknown elements $m_{00}^{\mathrm{SHG}}$, $m_{01}^{\mathrm{SHG}}$, $m_{02}^{\mathrm{SHG}}$ and $m_{03}^{\mathrm{SHG}}$ of the Mueller matrix, four independent incident polarization states are required. Let us consider four incident Stokes vectors, $S_{\mathrm{IN}}^{(i)}$ ($i = 1, 2, 3, 4$) such as: linear horizontal ($S_{\mathrm{IN}}^{(1)}$), linear vertical ($S_{\mathrm{IN}}^{(2)}$), linear at 45° ($S_{\mathrm{IN}}^{(3)}$) and right circular ($S_{\mathrm{IN}}^{(4)}$). Having taken into account the $\chi$ and $\psi$ of those polarization states, a $4 \times 4$ auxiliary matrix where each column $MS_{\mathrm{IN}}$ is one of the four vectors $S_{\mathrm{IN}}^{(i)}$ reaching the sample can be written as:

$$MS_{\mathrm{IN}} = \begin{pmatrix} S_{\mathrm{IN}}^{(1)} & S_{\mathrm{IN}}^{(2)} & S_{\mathrm{IN}}^{(3)} & S_{\mathrm{IN}}^{(4)} \end{pmatrix} = \begin{pmatrix} 1 & 1 & 1 & 1 \\ 1 & -1 & 0 & 0 \\ 0 & 0 & 1 & 0 \\ 0 & 0 & 0 & 1 \end{pmatrix}. \tag{A4}$$

The corresponding SHG intensity values emerging from the sample for those four incident polarization states are a result of:

$$\begin{pmatrix} \tilde{I}_{2\omega}^{(1)} & \tilde{I}_{2\omega}^{(2)} & \tilde{I}_{2\omega}^{(3)} & \tilde{I}_{2\omega}^{(4)} \end{pmatrix} = MC_{\mathrm{SHG}} \cdot MS_{\mathrm{IN}} \tag{A5}$$

with each $\tilde{I}_{2\omega}^{(i)}$ having the corresponding expression provided by (A2).

Finally, the elements of $MC_{\mathrm{SHG}}$ can be computed by means of a simple matrix inversion:

$$\begin{aligned} MC_{\mathrm{SHG}} &= \begin{pmatrix} m_{00}^{\mathrm{SHG}} & m_{01}^{\mathrm{SHG}} & m_{02}^{\mathrm{SHG}} & m_{03}^{\mathrm{SHG}} \end{pmatrix} \\ &= \begin{pmatrix} \tilde{I}_{2\omega}^{(1)} & \tilde{I}_{2\omega}^{(2)} & \tilde{I}_{2\omega}^{(3)} & \tilde{I}_{2\omega}^{(4)} \end{pmatrix} \cdot (MS_{\mathrm{IN}})^{-1}. \end{aligned} \tag{A6}$$

From these elements, different polarimetric parameters can be computed (as shown in equations (4)–(9)) and compared to the experimental ones in order to test the accuracy of the theoretical model here proposed (see section 3.2 of results).

## References


[1] Roth S and Freund I 1979 Second-harmonic generation in collagen *J. Chem. Phys.* **70** 1637–43

[2] Seeley R, Stephens T and Tate P 2003 *Anatomy and Physiology* (New York: McGraw-Hill)

[3] Williams R M, Zipfel W R and Webb W W 2005 Interpreting second harmonic generation images of collagen I fibrils *Biophys. J.* **88** 1377–86

[4] Stoller P *et al* 2003 Quantitative second-harmonic generation microscopy in collagen *Appl. Opt.* **42** 5209–19

[5] Lodish H *et al* 2000 *Molecular Cell Biology* (New York: Freeman W H)

[6] Hulmes D J S 2002 Building collagen molecules, fibrils, and suprafibrillar structures *J. Struct. Biol.* **137** 2–10

[7] Gusachenko I, Latour G and Schanne-Klein M C 2010 Polarization resolved second harmonic microscopy in anisotropic thick tissues *Opt. Express* **18** 19339–52

[8] Brasselet S 2011 Polarization-resolved nonlinear microscopy: application to structural molecular and biological imaging *Adv. Opt. Photon.* **3** 205–71

[9] Su I J *et al* 2011 Determination of collagen nanostructure from second-order susceptibility tensor analysis *Biophys. J.* **100** 2053–62

[10] Stoller P *et al* 2002 Polarization-dependent optical second-harmonic imaging of a rat-tail tendon *J. Biomed. Opt.* **7** 205–14

[11] Tuer A E *et al* 2011 Nonlinear optical properties of type I collagen fibers studied by polarization dependent second harmonic generation microscopy *J. Phys. Chem.* B **115** 12759–69
[12] Ávila F J, del Barco O and Bueno J M 2016 Polarization response of second-harmonic images for different collagen spatial distributions *J. Biomed. Opt.* **21** 066015
[13] Su P J *et al* 2009 Discrimination of collagen in normal and pathological skin dermis through second-order susceptibility microscopy *Opt. Express* **17** 11161–71
[14] Campagnola P J 2011 Second harmonic generation imaging microscopy: applications to diseases diagnostics *Anal. Chem.* **83** 3224–31
[15] Chang Y *et al* 2009 Theoretical simulation study of linearly polarized light on microscopic second-harmonic generation in collagen type I *J. Biomed. Opt.* **14** 044016
[16] Plocinik R M *et al* 2005 Modular ellipsometric approach for mining structural information from nonlinear optical polarization analysis *Phys. Rev.* B **72** 125409
[17] del Barco O and Bueno J M 2012 Second harmonic generation signal in collagen fibers: role of polarization, numerical aperture, and wavelength *J. Biomed. Opt.* **17** 045005
[18] Ávila F J, del Barco O and Bueno J M 2015 Polarization dependence of aligned collagen tissues imaged with second harmonic generation microscopy *J. Biomed. Opt.* **20** 086001
[19] Hristu R *et al* 2016 Improved quantification of collagen anisotropy with polarization-resolved second harmonic generation microscopy *J. Biophoton.* at press (https://doi.org/10.1002/jbio.201600197)
[20] Marsh D 1997 Dichroic ratios in polarized Fourier transform infrared for non-axial symmetry of $\beta$-sheet structures *Biophys. J.* **72** 2710–8
[21] Chen X *et al* 2012 Second harmonic generation microscopy for quantitative analysis of collagen fibrillar structure *Nat. Protocols* **7** 654–69
[22] Chipman R A 1995 Polarimetry *Handbook of Optics* 2nd edn (New York: McGraw-Hill)
[23] Mazumder N *et al* 2013 Stokes vector based polarization resolved second harmonic microscopy of starch granules *Biomed. Opt. Express* **4** 538–47
[24] Bancelin S *et al* 2014 Determination of collagen fiber orientation in histological slides using Mueller microscopy and validation by second harmonic generation imaging *Opt. Express* **22** 22561–74
[25] Kontenis L *et al* 2016 Second harmonic generation double Stokes–Mueller polarimetric microscopy of myofilaments *Biomed. Opt. Express* **7** 559–69
[26] Samim M, Krouglov S and Barzda V 2015 Double Stokes–Mueller polarimetry of second-harmonic generation in ordered molecular structures *J. Opt. Soc. Am.* B **32** 451–61
[27] Haupert L M and Simpson G J Chirality in nonlinear optics *Annu. Rev. Phys. Chem.* **60** 345–65
[28] Lee H *et al* 2013 Chiral imaging of collagen by second harmonic generation circular dichroism *Biomed. Opt. Express* **4** 909–16
[29] Chen X, Raggio C and Campagnola P J 2012 Second-harmonic generation circular dichroism studies of osteogenesis imperfecta *Opt. Lett.* **37** 3837–9
[30] Bueno J M *et al* 2004 Degree of polarization as an objective method of estimating scattering *J. Opt. Soc. Am.* A **21** 1316–27
[31] Ávila F J and Bueno J M 2015 Analysis and quantification of collagen organization with the structure tensor in second harmonic microscopy images of ocular tissues *Appl. Opt.* **54** 9848–54
[32] Bueno J M 2001 Measurement of parameters of polarization in the living human eye using imaging polarimetry *Vis. Res.* **40** 3791–9
[33] Bueno J M 2007 Polarimetry in the human eye using an imaging linear polariscope *J. Opt. A: Pure Appl. Opt.* **4** 553–61
[34] Bueno J M and Artal P 2007 Average double-pass ocular diattenuation using foveal fixation *J. Mod. Opt.* **55** 849–59
[35] Rao R A R, Mehta M R and Toussaint K Jr 2009 Fourier transform-second-harmonic generation imaging of biological tissues *Opt. Express* **17** 14534–42
[36] Aït-Belkacem D *et al* 2010 Influence of birefringence on polarization resolved nonlinear microscopy and collagen SHG structural imaging *Opt. Express* **18** 14859–70
[37] Mazumder N *et al* 2014 Revealing molecular structure and orientation with Stokes vector resolved second harmonic generation microscopy *Methods* **66** 237–45
[38] Aït-Belkacem D *et al* 2012 Microscopic structural study of collagen aging in isolated fibrils using polarized second harmonic generation *J. Biomed. Opt.* **17** 080506
[39] Latour G *et al* 2012 *In vivo* structural imaging of the cornea by polarization-resolved second harmonic microscopy *Biomed. Opt. Express* **3** 1–15
[40] Baum J and Brodsky B 1999 Folding of peptide models of collagen and misfolding in disease *Curr. Opin. Struct. Biol.* **9** 122–8
[41] Odin C *et al* 2008 Orientation fields of nonlinear biological fibrils by second harmonic generation microscopy *J. Microsc.* **229** 32–8